



Fabrication and tribological properties of the laser textured SiC cylinders with diamond coating

Enli Hu¹ · Jiaqi Zhi² · Yanxia Wu¹ · Shengwang Yu¹

Received: 3 December 2022 / Accepted: 24 February 2023 / Published online: 13 March 2023
© The Author(s), under exclusive licence to Springer-Verlag GmbH, DE part of Springer Nature 2023

Abstract

Laser surface texturing (LST) of silicon carbide (SiC) with the diamond coating (D/T-SiC) was studied in order to reduce friction and wear. The microstructure, morphology, and tribological properties of SiC substrate, textured SiC (T-SiC), and non-textured SiC with diamond coating (D/SiC) were also investigated for comparison. The samples modified by laser surface textured or fabricated with diamond coating (T-SiC, D/SiC, D/T-SiC) showed a conspicuous impact on reducing the friction and wear in dry friction, compared to SiC at various applied loads (5 N, 15 N, and 25 N). Additionally, the D/T-SiC showed lower friction coefficient and wear rate at all the conditions, especially, D/T-SiC reduced the friction coefficient of 79.7%, 84.8% and 86.2% compared to SiC, respectively, at applied loads of 5 N, 15 N and 25 N. The cylindrical textures were found to further reduce the friction coefficient by capturing abrasive, which decrease the width and depth of scratch of diamond coating. Furthermore, the diamond coating could decrease the deformation of cylindrical textures. Besides, a small amount of transition from diamond to sp^2C at the counterface improved tribological properties. This work provides valuable guidance for SiC modification.

Keywords SiC · Laser fabrication · Diamond · Friction

1 Introduction

Since high-performance abrasive tools are urgently needed in ultra-high-precision processes characterized by intense load and high temperature, the selection of abrasive tools is essential to ensuring the accurate fabrication of workpieces [1]. Silicon carbide (SiC) is an excellent ceramic material due to its exceptional characteristics, such as abrasive resistance, corrosion resistance, and high thermal conductivity. The SiC ceramic has been extensively applied in abrasive, bearings mechanical seals as well as other fields [2–4]. However, with impact or large load, the brittle splintering characteristics, the surface of abrasives and polished components will be severely damaged by grinding and polishing

performance [5]. To address the issue, several strategies are employed. Amongst them, the surface texturing is frequently tailored to increase the mechanical and tribological capabilities.

Surface texturing has been widely used to significantly reduce the friction coefficient, contributing to the practical improvement of wear resistance, due to the exceptional characteristics, such as anti-friction and anti-adhesion effects [6–8]. Amongst them, the texture patterns which are applied by laser fabrication are the most widely used in surface texture processing [9]. By adjusting the various parameters during laser fabrication, such as the shape, size, etc., the tribological characteristics of SiC can be easily controlled [10, 11]. Tshabalala et al. [12] found that the pulse energy and lateral overlaps increased logarithmic material removal during surface texturing. Antoszewski et al. [13] used a diode-pumped Nd: YAG laser to generate micropores on the ring surface of SiC, and found frictional property was improved compared to the surface without texture. Orlova et al. [14] processed the nanosecond pulsed laser to create the surface texture on the SiC ceramic and found the texture SiC could reduce friction coefficient by about 20%, compared to

✉ Yanxia Wu
haifengwuyu@126.com

✉ Shengwang Yu
yushengwang@tyut.edu.cn

¹ College of Materials Science and Engineering, Taiyuan University of Technology, Taiyuan 030024, China

² Beijing Huajin Wanshun Machinery Co., Ltd, Beijing 100025, China

the unprocessed surface. Although the laser texture can improve its tribological properties, it was still brittle and maintain a high wear rate, limiting its potential application. Furthermore, the laser texture patterns are always inlaid on the surface, few reports introduce the raised micro-structures on the surface.

In order to overcome the shortcoming of surface texture, surface coating is fabricated to enhance the tribological property and prolong the texture life. Diamond coating is a striking material with high mechanical hardness, wear resistance, low frictional coefficient, high elastic modulus, and high thermal conductivity, which can be used in various industries [15–17]. The coating has been extensively applied in cutting tools, molds, bearings, and various seals. Furthermore, accompanied by the high bonding force between diamond and SiC [18], compared to nano-diamond and micro-nano-multilayer diamond, the micro-diamond have a higher abrasive resistance, low wear rate and bonding force, respectively. Therefore, fabrication of textured SiC with micro-diamond coating can acquire synergism, achieving high hardness and low friction and wear, and shows a potential application in abrasive fields.

Bearing these in mind, a textured SiC by laser processing and modified with diamond (D/T-SiC) coating was a method to improve its tribological properties. In comparison, SiC, texture SiC (T-SiC), and diamond/SiC (D/SiC) were investigated under the same conditions. The structure, morphology, and tribological properties under different applied loads are analyzed. Additionally, the tribological mechanism related to them was discussed.

2 Materials and methods

2.1 Laser surface texturing and diamond coating deposition

The hot-press sintered SiC ceramics with the dimensions of 12 mm × 12 mm × 7 mm were employed as substrate materials that had a root mean square surface roughness (Sq) value of about 0.57 μm . After ultrasonic cleaning for 10 min in alcohol and acetone, all specimens were used after drying with hot air. The fiber laser was activated by Nd: YAG, the wavelength was 1080 nm, and equipped with a 180 mm focusing lens was used to produce cylindrical texture on the surface of the SiC substrate. The related experimental parameters were: Laser power was 12 W, the frequency was 20 kHz and curving speed was 200 mm/s. The cylindrical texture with a diameter and spacing of 250 μm and thickness of 60 μm was produced on the surface with a Sq of about 0.59 μm .

Then, the substrates were cleaned by H plasma in the cavity of microwave plasma chemical vapor deposition equipment (TYUT-MPCVD) [19] and then deposited on the diamond coating. A gas mixture of H_2 and CH_4 (flow rate of 400 sccm and 60 sccm, respectively) was used for the deposition of the diamond coating. The microwave power and the deposition pressure were 3 ± 0.2 kW and ~ 17 kPa respectively. The temperature of the substrates was maintained at 750 ± 5 °C to avoid graphitization and the duration of deposition time was 10 h. The resulting textured SiC with diamond coating was recorded as D/T-SiC, and its schematic diagram of the fabrication process is shown in Fig. 1. For comparison, the bare SiC substrate

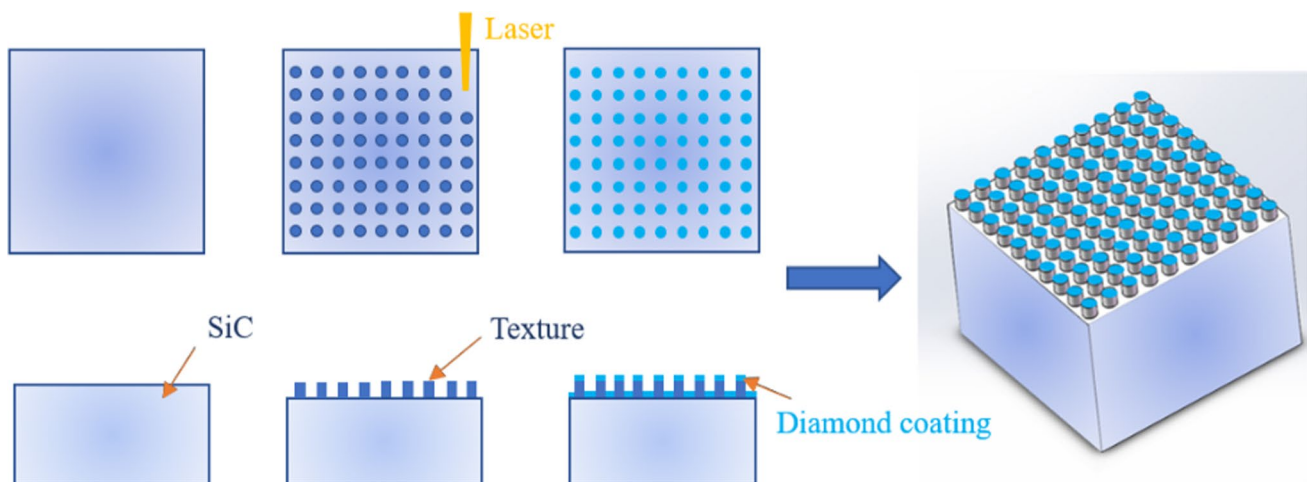


Fig. 1 Schematic diagram of fabrication process of textures and diamond deposition on SiC ceramic

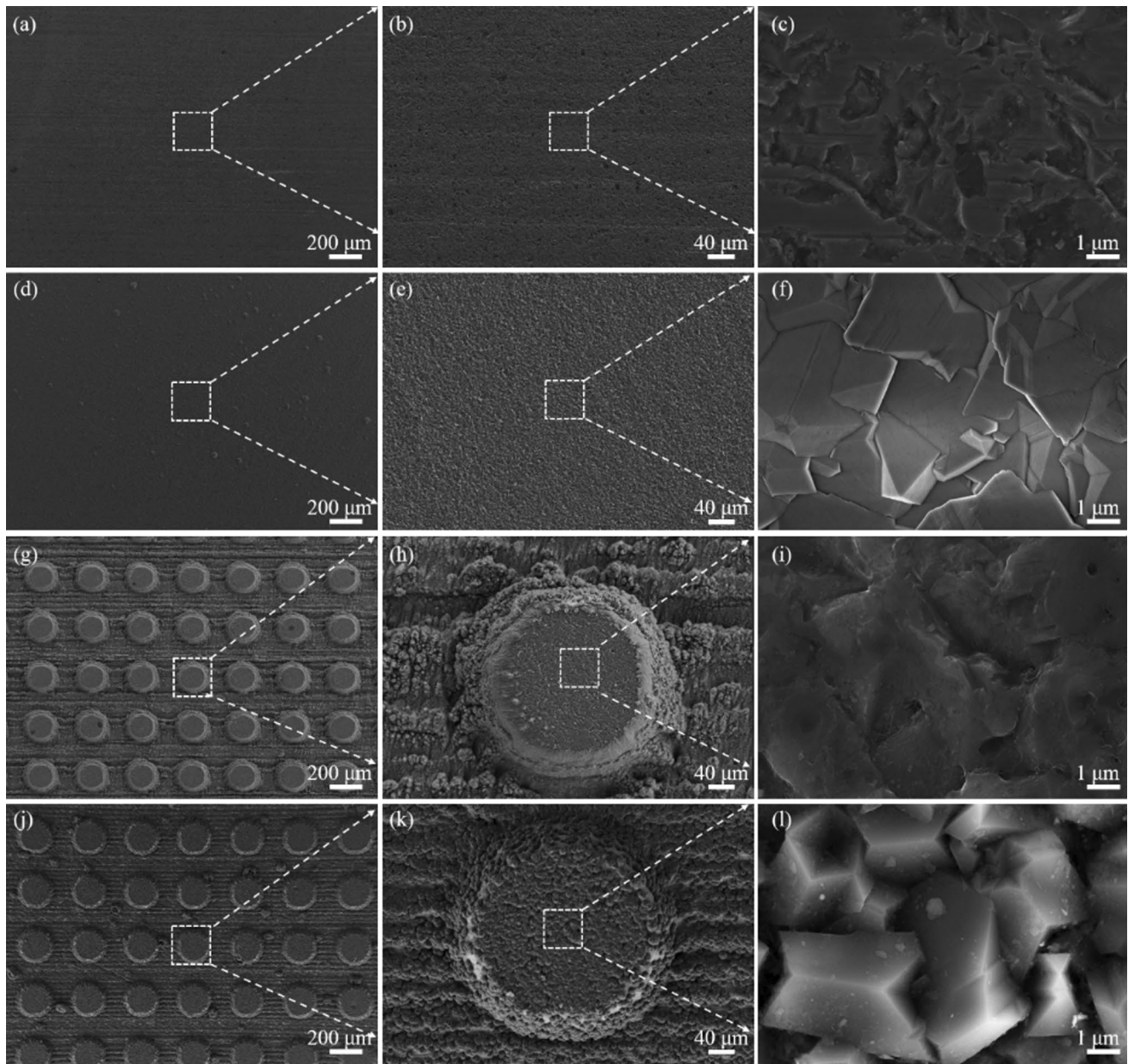


Fig. 2 The morphologies of SiC (from **a** to **c**), D/SiC (from **d** to **f**), T-SiC (from **g** to **i**), and D/T-SiC (from **j** to **l**)

without texture but the deposited diamond was recorded as D/SiC. Additionally, the textured SiC substrate without diamond deposition was recorded as T-SiC.

2.2 Microstructure characterization

The surface morphologies and crystal size of the diamond coating were analyzed by scanning electron microscopy (SEM, Zeiss-Gemini 300) coupled with an energy dispersive spectrometer (EDS, Oxford). The crystallographic orientation of SiC and diamond coating were characterized by X-ray diffraction (XRD, Rigaku). The crystalline quality

of SiC and diamond coating were analyzed by Renishaw Invia Raman microscope with the following condition: laser source of Diode Pumped Solid State laser (DPSS), laser excitation wavelength of 532 nm (25mW) and laser power of 25%. The three-dimensional images and surface toughness of different specimens were observed by optical microscope (VHS-6000, Keyence).

2.3 Friction test

Reciprocating ball-on-flat sliding tribometer (UMT-TriboLab, Bruker) was used to evaluate the friction and wear

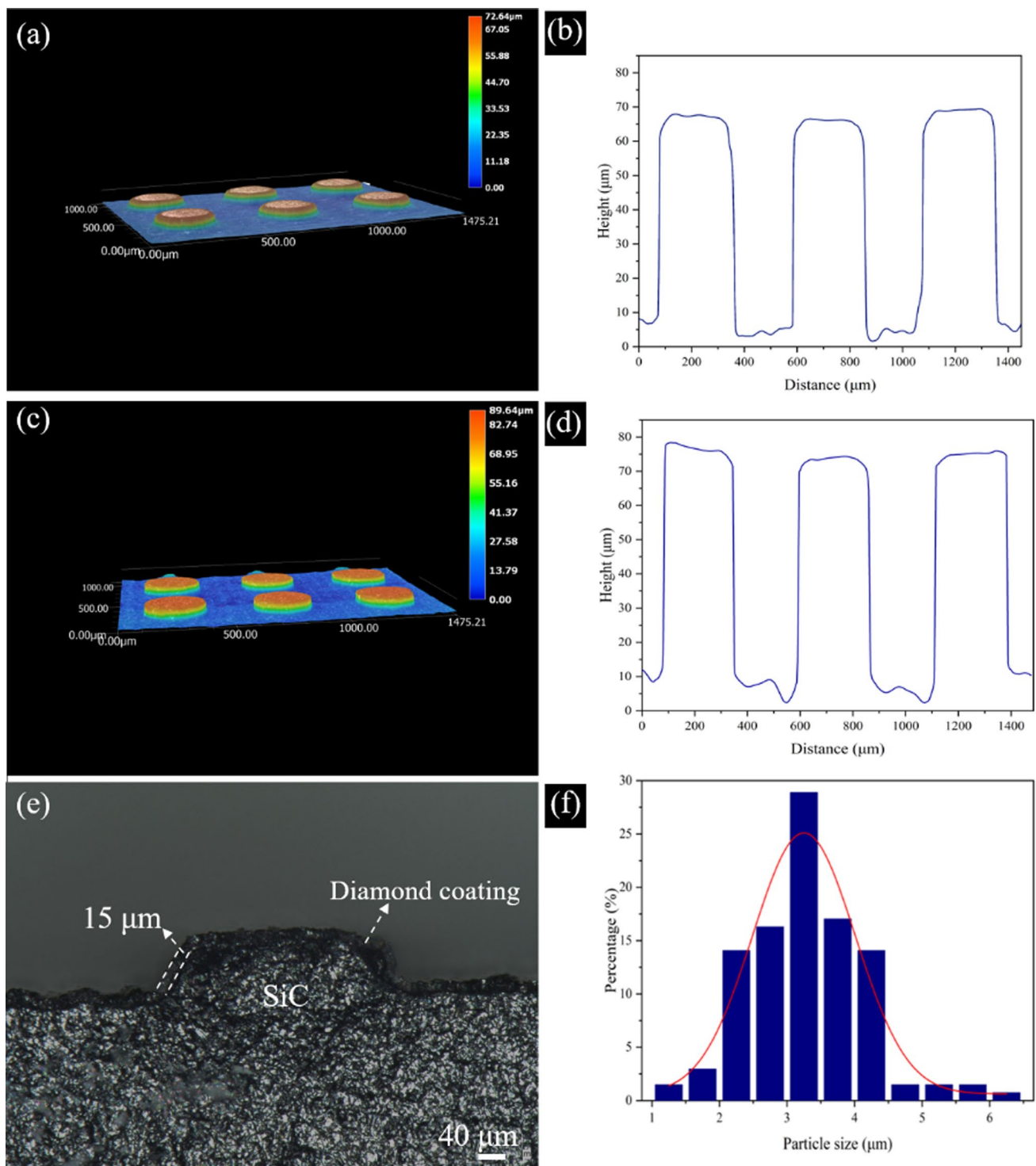


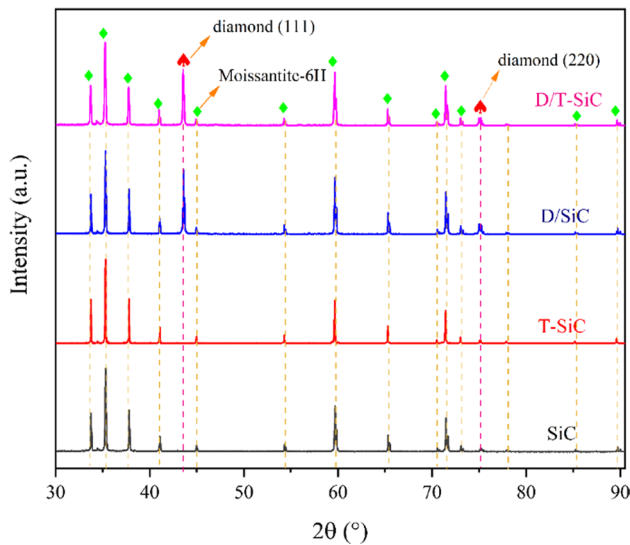
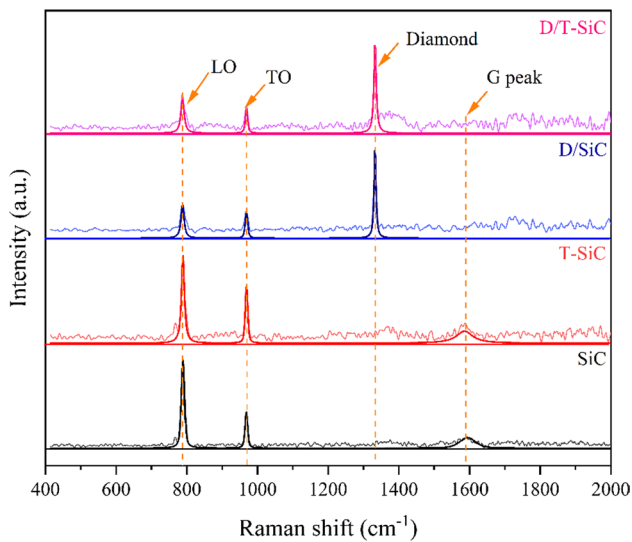
Fig. 3 The optical three-dimensional images and the curves of cross-section of T-SiC (from **a** to **b**), D/T-SiC (from **c** to **d**) and a cross-sectional morphology (**e**) with diamond crystalline distribution on the hill of D/T-SiC (**f**)

performances in dry friction. The Si_3N_4 ball with a diameter of 10 mm and a hardness of 70 HRC was employed as the counterpart. The friction tests were performed with the normal load of 5 N, 15 N, and 25 N, respectively. The

reciprocated move speed frequency (f) was 2 Hz, the sliding length of 4 mm, and the sliding time of 5400 s, at room temperature and repeated three times. Ahead of the friction tests, both specimen and counterpart balls were cleaned with

Table 1 The surface roughness of different specimens

Specimen	Root mean square roughness Sq (μm)	Average roughness Sa (μm)
SiC	0.57 ± 0.02	0.49 ± 0.02
D/SiC	1.14 ± 0.09	1.04 ± 0.03
T-SiC	0.59 ± 0.09 (on the hill) 1.08 ± 0.09 (in the valley)	0.47 ± 0.06 (on the hill) 0.89 ± 0.07 (in the valley)
D/T-SiC	1.14 ± 0.09 (on the hill) 2.17 ± 0.09 (in the valley)	0.97 ± 0.04 (on the hill) 1.99 ± 0.06 (in the valley)

**Fig. 4** The XRD diffraction of SiC, T-SiC, D/SiC, D/T-SiC**Fig. 5** The Raman spectrum of SiC, T-SiC, D/SiC, D/T-SiC

acetone in the ultrasonic bath to remove the impurities for capturing accurate data. The statistics of friction curves were gained directly from the tribometer. The wear morphologies

of the surface were analyzed by SEM and the dimensions of wear track were measured by optical microscope (VHS-6000, Keyence) and the specific wear volumes were computed based on these profiles. For the wear traces of different specimens, three profiles were recorded and the results were averaged. Based on the value of the volume loss, the specific wear rate (k) was computed using Archard's equation [20], $k = V/F_n \times s$ (mm^3/Nm), where k is specific wear rate ($\text{mm}^3\text{N}^{-1}\text{m}^{-1}$), V is the wear volume (mm^3), F_n is the normal load (N) and s is sliding length (m). Moreover, the corresponding element dispersion was presented by EDS. The changes in the composition and structure of the C element on the Si_3N_4 ball were observed by Raman.

3 Results and discussion

3.1 Microstructural and morphology

The surface morphologies of SiC, T-SiC, D/SiC, and D/T-SiC are presented in Fig. 2. The surface of the SiC substrate existed some irregular holes distributed uniformly (Fig. 2a–c). The morphology of D/SiC had a relatively dense diamond coating (Fig. 2d–f). After laser texturing, there were parallel stripes across the surface of T-SiC caused by the laser etching (Fig. 2g–i). The morphology of the diamond grown on the hill of D/T-SiC was relatively compact. The spacing between adjacent cylinders was not significantly different after the diamond deposition (Fig. 2j–l). The diamond on the valley grew linearly, due to the diamond preferred to nuclearize and grow on the stripes which were the residual remains fabricated by the laser, and the lateral surface had a sparse diamond, due to the edge effect [21] of the superficial edge of texture and the distinction of the composition of C-H plasma group between the hill and the valley.

The three-dimensional images, the cross-sectional profile and the height of the textured specimens (T-SiC, D/T-SiC) with diamond crystalline distribution on the hill of D/T-SiC are shown in Fig. 3. The stereoscopic morphologies of the textured specimens before and after depositing diamond coating are shown in Fig. 3a and c. The textured cylinders fabricated by laser abscission obtained uniform arrangement

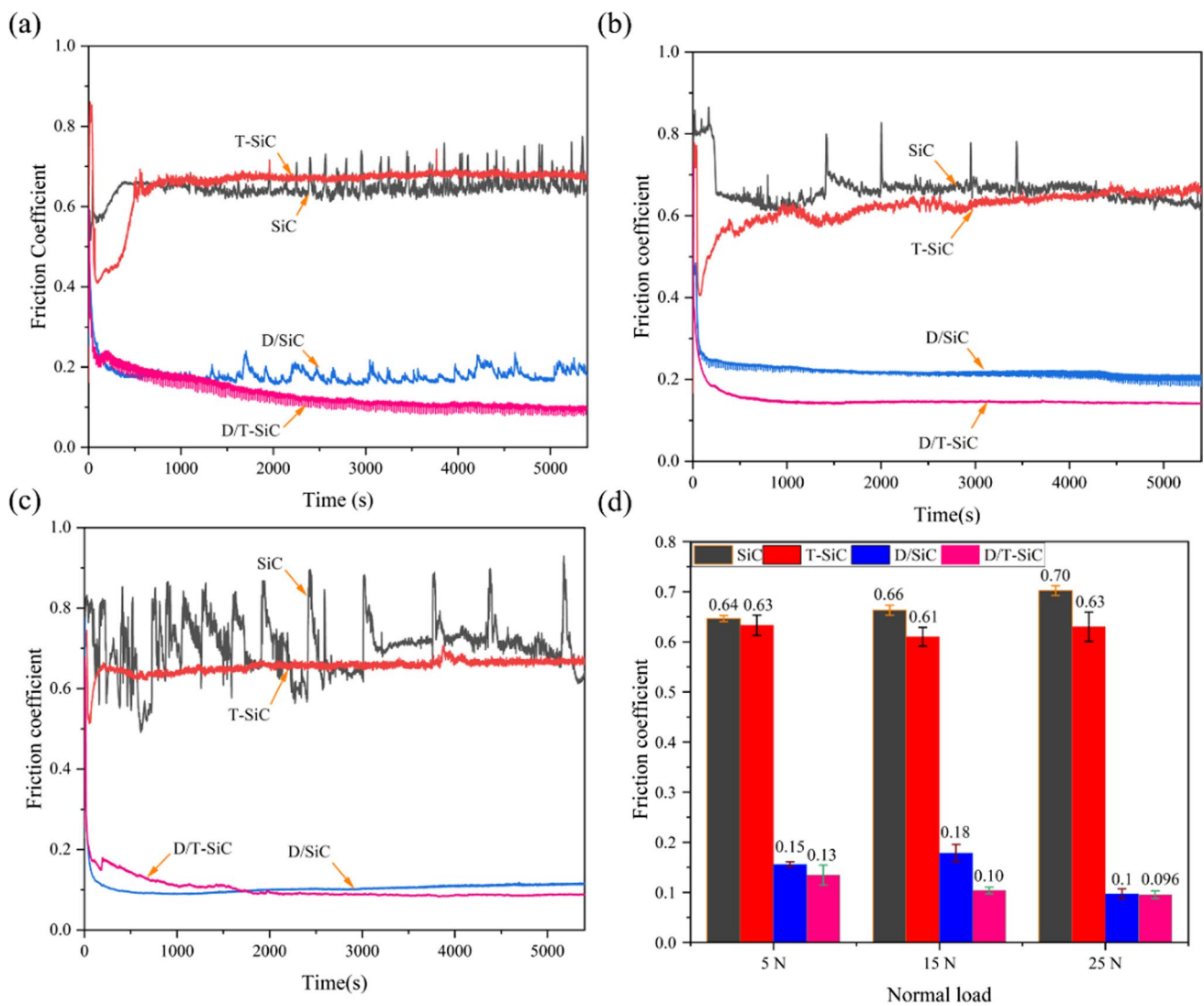


Fig. 6 Friction coefficient of different specimens varies with loads (a at normal load of 5 N, b at normal load of 15 N, c at normal load of 25 N, and d the average friction coefficient)

with clear morphologies. The diamond coating was visible in the cross-sectional morphology of D/T-SiC, as shown in Fig. 3e. The diamond coating grown on the boundary of the texture was compact and successive without obvious defects and impurities with a thickness of about 15 μm . The distribution of grain size on the hill of D/T-SiC showed the distribution of the size of grain corresponded to a normal distribution, with an average grain size of about 2.7 μm (Fig. 3d). Figure 3b, d presents the height of T-SiC and D/T-SiC were about 60 μm , and 75 μm with a distance of about 250 μm . Due to a higher roughness of the valley produced by the laser fabrication, compared to the roughness of the hill of texture ($S_q = 1.14 \mu\text{m}$), the diamond in the valley and side was more disordered ($S_q = 2.17 \mu\text{m}$).

The surface roughness parameters of different specimens are obtained by the micrographs in Fig. 3 and are presented in Table 1.

The XRD diffraction patterns of SiC, T-SiC, D/SiC, and D/T-SiC are shown in Fig. 4. The Moissanite-6H was the main composition of T-SiC as same as the original SiC specimen [22]. It indicated that there was no visible phase transformation between the substrate material and the textured specimens after the laser fabrication. It could be seen that the diamond coating had not changed the composition of SiC in the depositional duration of the D/SiC and D/T-SiC. The coating exhibited two typical peaks at 43.8° , and 75.3° , which were assigned to the (111) and (220) planes of diamond. The diffraction peak intensity of (111) was higher

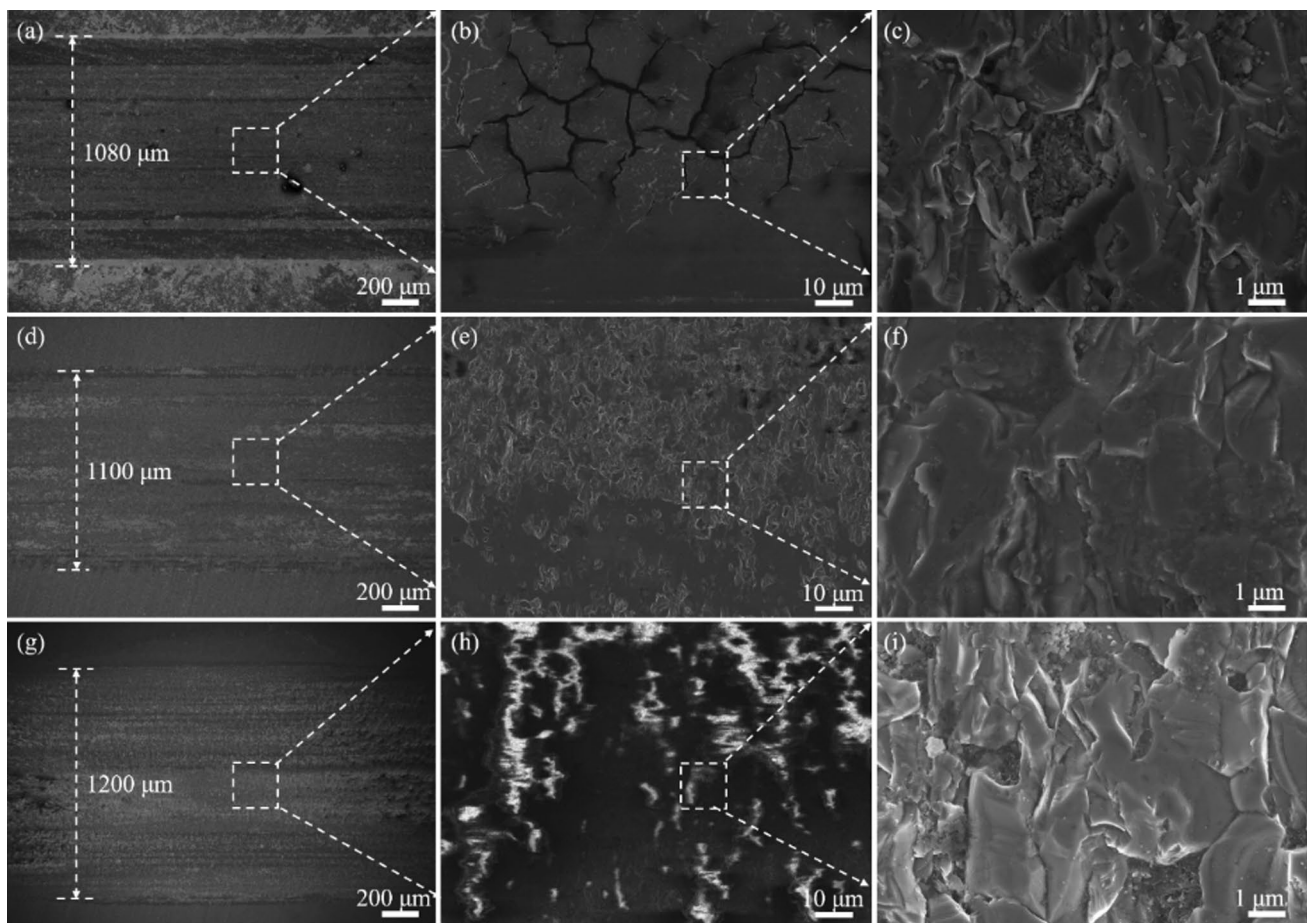


Fig. 7 The morphologies of SiC after friction and wear (**a–c** at normal load of 5 N, **d–f** at normal load of 15 N, **g–i** at normal load of 25 N)

than the (220) in D/SiC and D/T-SiC with a ratio of about 18 and 20. It indicated the diamond crystal preferred to grow the diamond with the (111) plane and the diamond orientation was not affected by the laser surface texture.

The Raman spectroscopy with an excitation wavelength of 532 nm was used to characterize the substrate and coating further, as shown in Fig. 5. The characteristic peaks were located nearly at 790 cm^{-1} , and 970 cm^{-1} , corresponding to transverse optical (TO) and longitudinal optical (LO) phonons of 6H-SiC [23]. The peaks located at 1580 cm^{-1} of SiC and T-SiC were the G peak. The graphite as a sintering additive was put in hot sintering of SiC, and the incomplete reactional graphite was detected by Raman as the G peak. The Raman spectra of the original and laser-textured specimens obtained similar characteristics and intensity. The quality of texture was unaffected in the duration of laser fabrication. The decreasing peak intensity at 790 cm^{-1} and 970 cm^{-1} in the D/SiC and D/T-SiC indicated that the diamond coating was deposited on textured surface, resulting in a reduction of the Raman signal of SiC. The sharp peaks between the D/SiC and D/T-SiC located at 1333.2 cm^{-1} and 1333.6 were

diamond phases [24], the sharp Raman intensity and without any other peak, respectively.

3.2 Tribological properties

The frictional curves of SiC, T-SiC, D/SiC, and D/T-SiC against Si_3N_4 ball at different applied loads (5 N, 15 N, and 25 N) are shown in Fig. 6. As presented in Fig. 6a, the friction coefficient curves of textured specimen and original SiC specimen exhibited the similar trend. The friction coefficient of SiC fluctuated at applied load of 5 N during the steady period. The friction coefficient curve of T-SiC decreased dramatically at the initial stage, then kept stable at about 0.63. Due to the high wear resistance of diamond coating modified on the surface [25], specimens coated with diamond (D/SiC, D/T-SiC) had lower friction coefficient compared to the samples without diamond coating (SiC, T-SiC). The friction coefficient of D/SiC at normal load of 5 N was about 0.22, and the friction coefficient of D/T-SiC showed lower and steadier friction coefficient of 0.15. Figure 6b demonstrates the variation curves of different specimens at

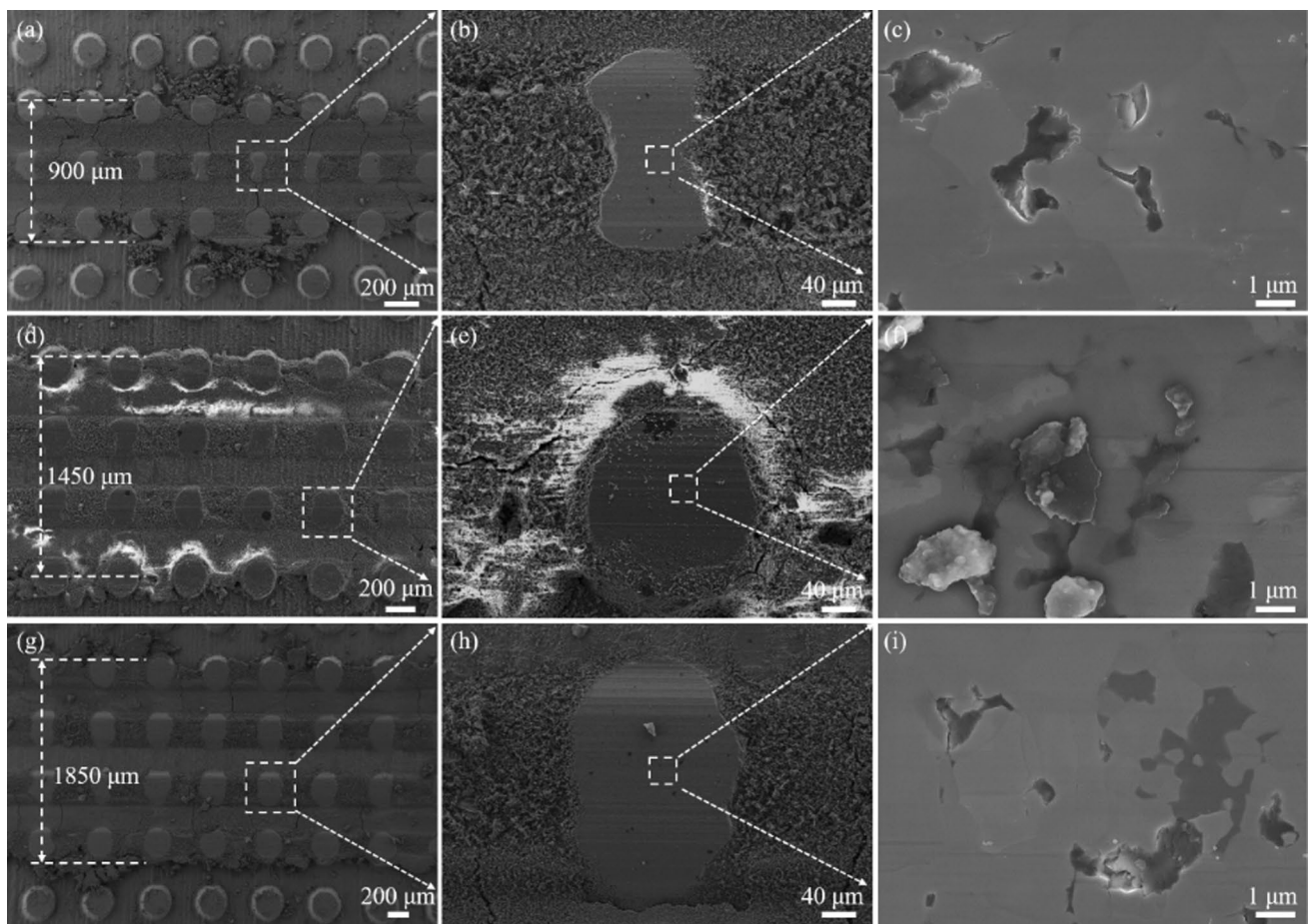


Fig. 8 The morphologies of T-SiC after friction and wear (**a–c** at normal load of 5 N, **d–f** at normal load of 15 N, **g–i** at normal load of 25 N)

normal load of 15 N, it showed a comparable tendency as shown at the normal load of 5 N. Figure 6c illustrates the variation curves of the friction coefficient in 25 N. The friction coefficient and the fluctuation extent of SiC increased dramatically without a steady stage. The friction coefficient curves of T-SiC changed slightly with increasing the applied load further to 25 N. The friction coefficient of other specimens changed little with increasing applied load. Based on the friction coefficient of different specimens, the relation between the friction coefficient and contact area was given in the following formula. According to the frictional definition [26]

$$\mu = F_f / F_n, \quad (1)$$

where μ is the friction coefficient, F_f is the frictional force, F_n is the normal force on the specimen. Combined with Binomial law of friction, the equation is easily acquired as follow, [27]

$$\mu = \alpha A / F_n + \beta, \quad (2)$$

where α , β are the factors related to physical and mechanical properties on the frictional surface, A is the actual contact surface, F_n is the normal load. Because of the textured circular blocked, when the counterpart ball was sliding on the surface of the specimens, there were many gaps in micro-scale between the blocks, which decreased the actual contact area and thus the average frictional coefficient.

The average friction coefficient of specimens with different loads (5 N, 15 N and 25 N) are presented in Fig. 6d. It was observed that different specimens at the normal load of 5 N, the T-SiC reduced the friction coefficient of 1.5–11.4%, compared to SiC specimen, the specimens with diamond coating (D/SiC, D/T-SiC) could reduce the friction coefficient of 46.1–76.9% compared to these without diamond coating (SiC, T-SiC), especially, the D/T-SiC reduced the friction coefficient of 76.9% compared to SiC. Furthermore, the friction coefficient reduction of D/T-SiC at applied load of 25 N showed the best efficiency of 85.7–86.2% compared to SiC. It was observed that diamond played greater impact on the friction coefficient than texture. It was attributed to

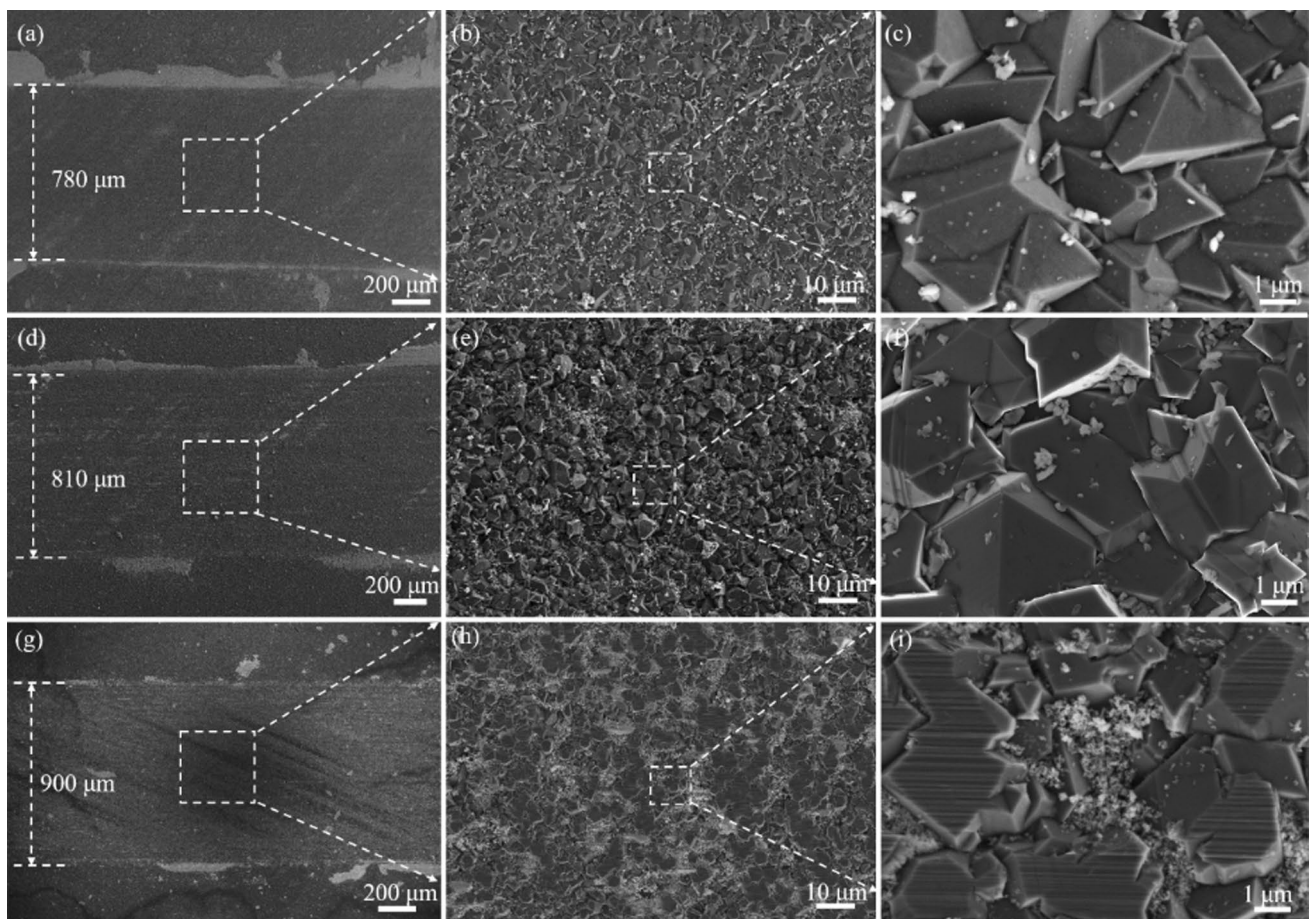


Fig. 9 The morphologies of D/SiC after friction and wear (a–c at normal load of 5 N, d–f at normal load of 15 N, g–i at normal load of 25 N)

the fact the normal load increased the edge stress of D/T-SiC, which produced the coating peeling.

3.3 Wear morphologies and mechanism

Figure 7 shows the wear morphology of the SiC at various applied loads (5 N, 15 N, and 25 N). There were spalling debris with brittle cracks at applied load of 5 N. The cracks disappeared and the wear debris was flattened at applied load of 15 N. There was a deep indentation at applied load of 25 N. SiC kept fracturing continuously because of the normal load exceeded the compressive strength [28]. More debris in the wear track led to the obvious fluctuation of frictional curve as shown in Fig. 6c.

Figure 8 shows the wear morphology of T-SiC at various loads (5 N, 15 N, and 25 N). Figure 8a–c shows the edge of the cylindrical texture was ground brittle under the normal load of 5 N [29], due to the micro-crack in the brittle material caused by the coupling effect of load and sliding in the reciprocating movement [30]. The texture appeared to deform in the vertical and horizontal direction without

identified cracking at applied load of 15 N. The reason was deformation of the texture caused by dislocation and micro-crack produced by excessive load and movement of the counterpart ball [31]. Especially, more obvious deformation appeared at the edge at applied load of 25 N (as shown in Fig. 8g–i) caused by too high edge stress concentration [32].

Figure 9a–c shows the morphology of D/SiC after the frictional test at various load. The surface of the diamond coating had sharp edges without apparent grinding cracks and scratches at applied load of 5 N. The whole diamond coating was not blunt visibly at applied load of 15 N except for the edge of the diamond crystal. However, the diamond coating was worn out and flattened with the typical morphology of abrasive wear at applied load of 25 N.

Figure 10a–c presents the edge of diamond coating on D/T-SiC exhibited slight abrasion at applied load of 5 N [33]. The scratch on the diamond coating edge was more obvious at applied load of 15 N. Additionally, it was extended from edge to center at applied load of 25 N, which was caused by the stress concentration of the texture. Some spalling mainly appeared on the edge of the diamond surface, and some scratches appeared on the center of the diamond with

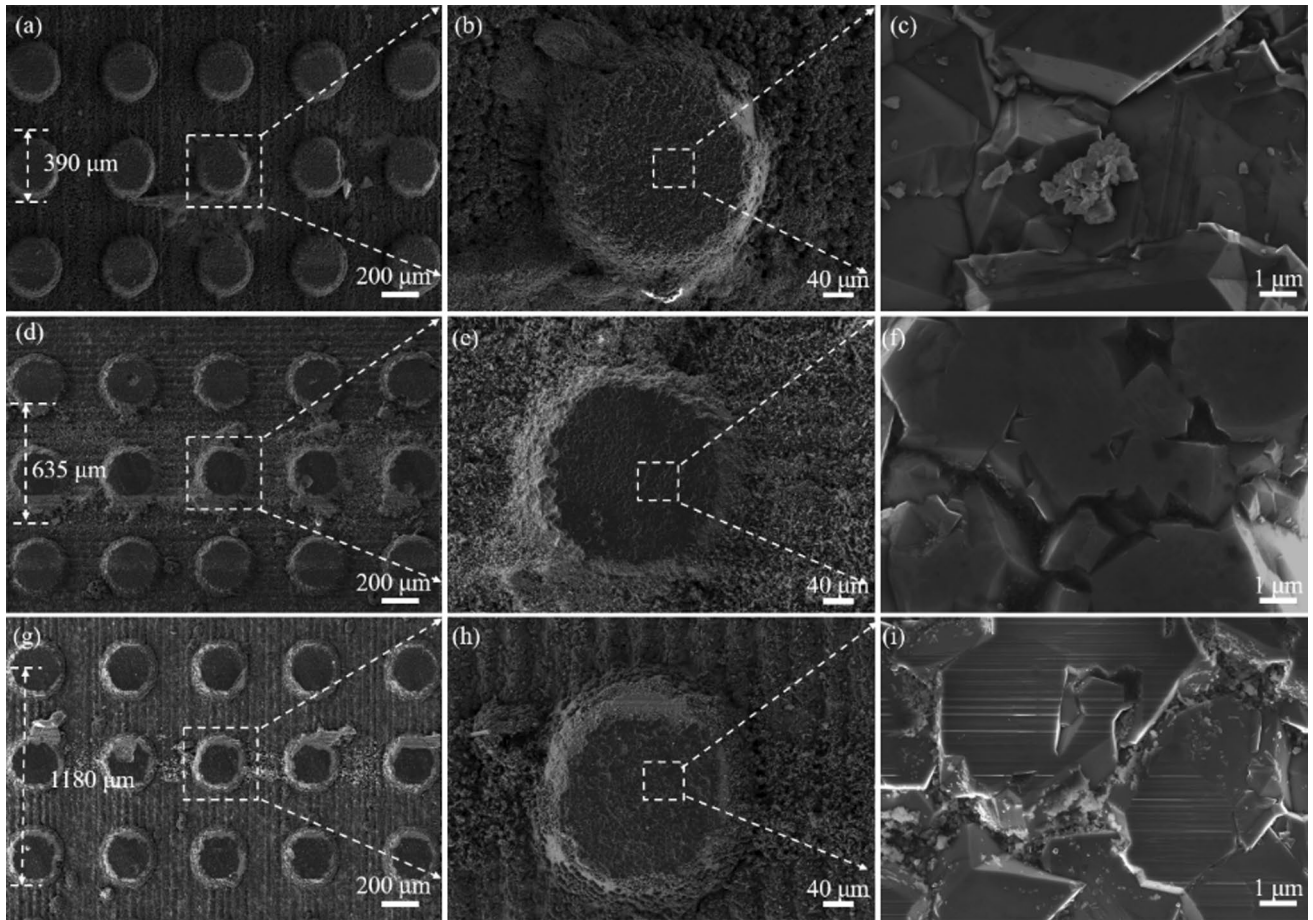


Fig. 10 The morphologies of D/T-SiC after friction and wear (a–c at normal load of 5 N, d–f at normal load of 15 N, g–i at normal load of 25 N)

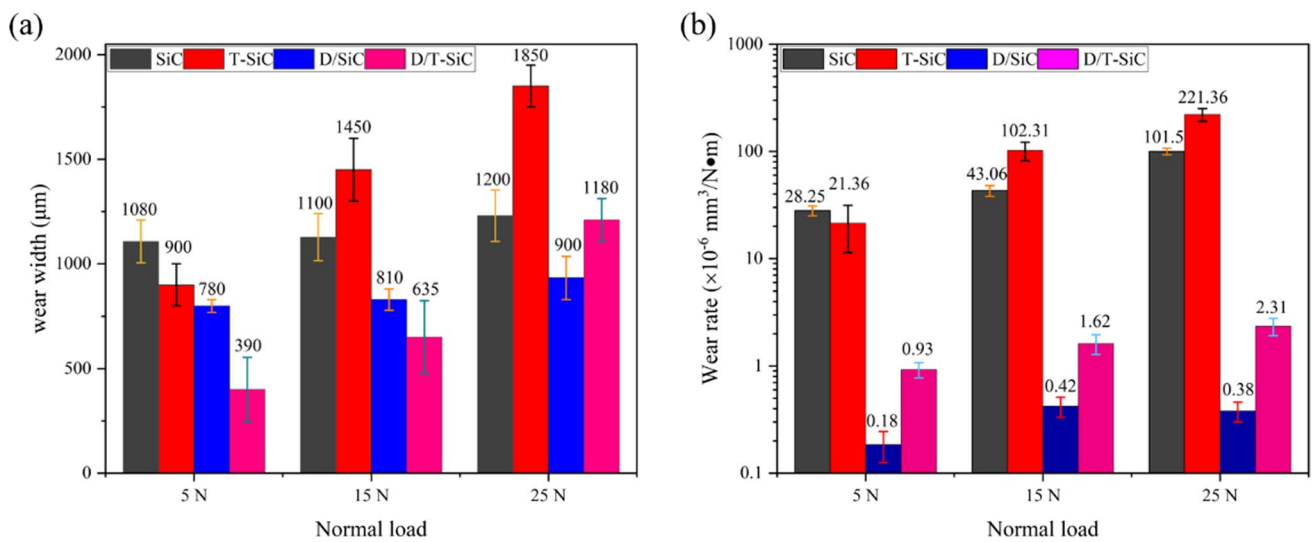


Fig. 11 The wear widths and wear rates of different specimen varied with loads (5 N, 15 N and 25 N)

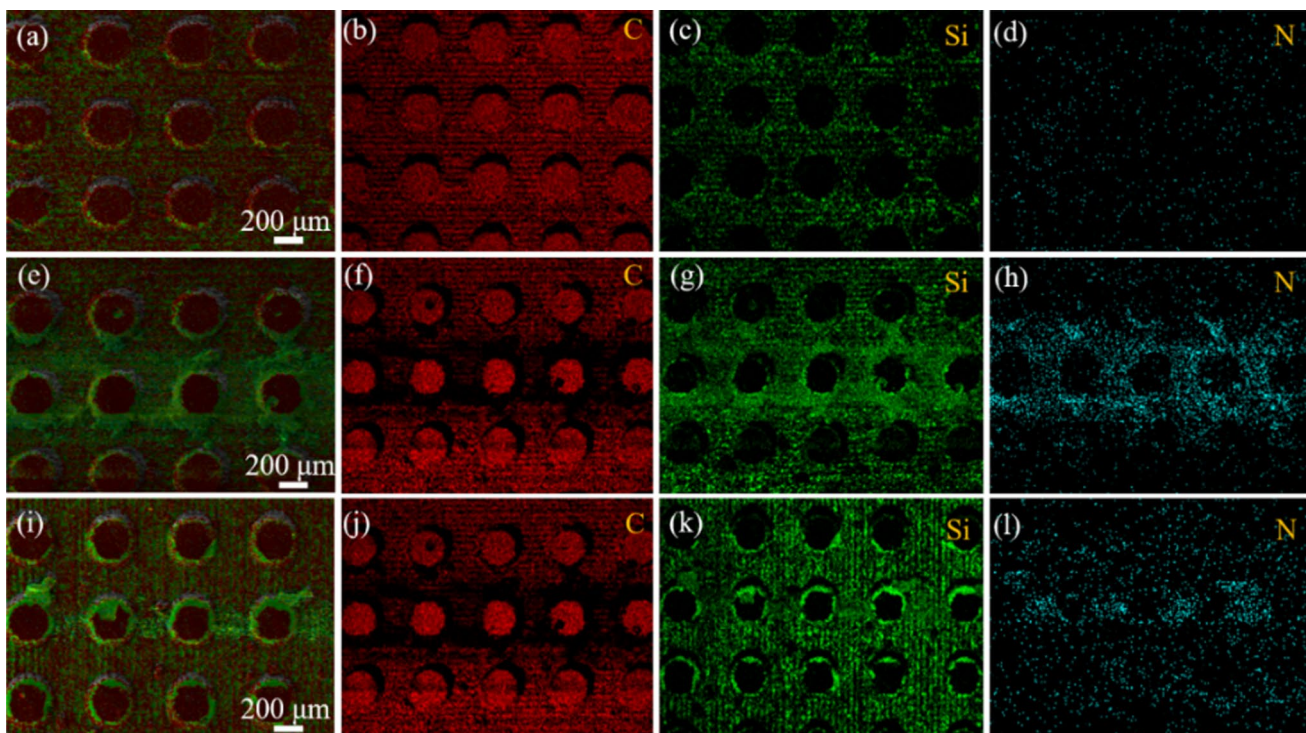


Fig. 12 The EDS element analysis of D/T-SiC after friction and wear (from **a** to **d** at applied load of 5 N, from **e** to **h** at applied load of 15 N, from **i** to **l** at applied load of 25 N)

no clear damage. Excessive loading made the diamond coating crack even though the coating was worn out with slight deformation of the substrate. Besides, the abrasive wear was more serious on the surface, compared to that the applied load of 15 N.

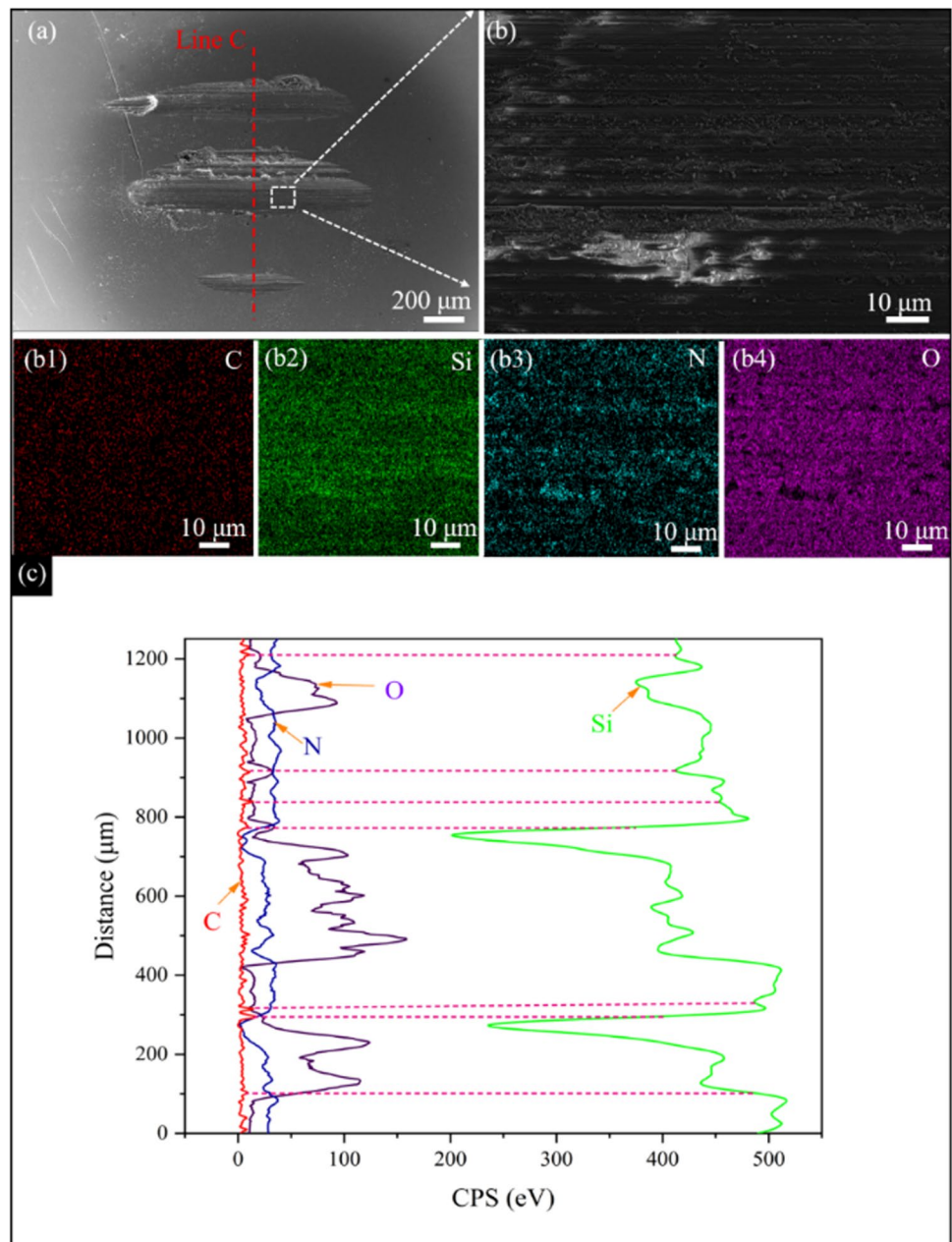
Figure 11a shows the variation in wear width of different specimens at varied loads (5 N, 15 N, and 25 N). The wear width of all specimens increased with the load rising because of increased contact surface. Besides, the high hardness of diamond can resist the deformation and wear width. Figure 11b illustrates the corresponding wear rates of the specimens varied with load. The wear rates of the specimens coated with diamond coating (D/SiC, D/T-SiC) were significantly decreased. The textured specimens (T-SiC, D/T-SiC) had higher wear rates due to the increasing contact and edge stress concentration. The surface texture modified with diamond coating could remarkably decrease friction coefficient and wear rate compared to the uncoated SiC.

The corresponding EDS results of wear track on the D/T-SiC at various applied loads (5 N, 15 N, and 25 N) are presented in Fig. 12. It could be seen that the wear of the diamond coat increased with increasing load, and high contents of Si and N due to the low hardness of the Si_3N_4 ball compared with the diamond coating. The wear morphology and element distribution of C, Si, N, and O in the Si_3N_4 counterpart ball sliding against D/T-SiC at applied load of 15 N is

given in Fig. 13. It confirmed the above result. Furthermore, Si decreased inside the scratches and increased outside the scratches. While the dispersion of C and O showed the contrary trends compared to Si, it increased inside the scratches and decreased outside the scratches. The element of C was transferred from diamond coating to the scratches of the counterpart by abrasive action.

The corresponding Raman spectrum of the scratch on the Si_3N_4 ball and D/T-SiC are shown in Fig. 14. It could be seen that the D/T-SiC specimen after the frictional test appeared an obvious peak called ν peak at 1450 cm^{-1} which was related to the sp^2 carbon in the grain boundary [34]. The diamond peak on the scratch broadened, compared to the diamond peak on the specimen. Besides, at 1580 cm^{-1} appeared an obvious G peak which was related to graphite. The diamond phase was tending to transfer to sp^2 C in the tribological test on the Si_3N_4 ball. On the contrary, the transformation was not observed on the D/T-SiC, the ν peak which was related to sp^2 C at grain boundary appeared after the tribological test. That was due to the continuous load force and contact area at the counterface, which accumulated more energy and caused the transition of the diamond phase, and the transformation made it easier to be transferred to the surface of the Si_3N_4 ball. Therefore, the heating and shearing under loads could provide enough activation energy for the phase change from sp^3 C to sp^2 C [35]

Fig. 13 The morphology and corresponding EDS spectrum of the counterpart ball sliding against D/T-SiC at applied load of 15 N after the tribological test



In summary, the different wear mechanisms existing in the specimens with texture and diamond coating in the frictional tests are shown in Fig. 15. As shown in Fig. 15a, the SiC exhibits a smooth indentation in loads with brittle cracking due to the wear debris moving with the counterpart ball, has an abrasive polishing effect. Figure 15b presents the tribological mechanism of T-SiC, the texture has the effect of debris capturing, and reduces the friction coefficient. However, the textured cylinders grind brittlely and break in low load. The textured cylinders deform with the load increasing, due to the

edge stress concentration and the development of microcracks under loads. Figure 15c shows the tribological mechanism of the D/SiC, the wear resistance and low friction coefficient of diamond reduce the adhesive force on the contact surface and the deformation of SiC substrate. Owing to the presence of diamond coating, the D/SiC exhibits slight bluntness in small loads, and the scratches emerged when the embedded debris was sliding with the counterpart ball, especially at large loads. Compared to the SiC, D/SiC, and T-SiC, the D/T-SiC obtains the advantages of surface texture and diamond coating,

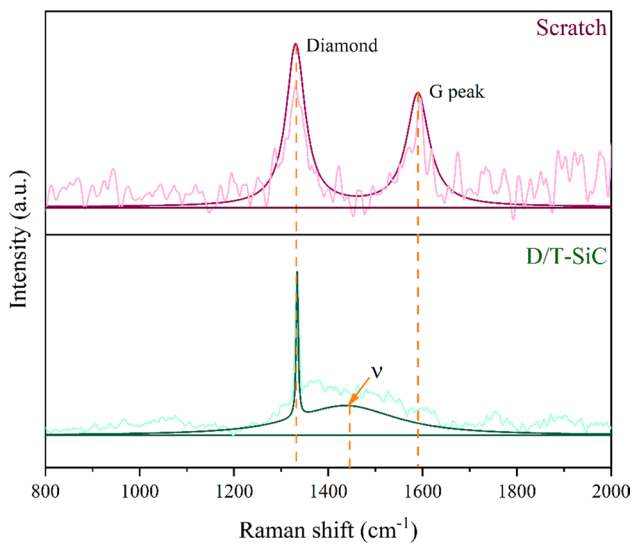


Fig. 14 The Raman spectrum of the scratch on Si₃N₄ ball and D/T-SiC specimen

protects the surface of SiC, and improves tribological property (as shown in Fig. 15d). Furthermore, the laser surface texture with diamond coating avoids the deformation of SiC, and alleviates the abrasive scratches. The mechanism of D/T-SiC avoided the deformation of SiC: the high grain boundary binding force and flexural strength of polycrystalline diamond coating prevent the crack of textured specimens [36], the low

friction coefficient of diamond coating can rapidly reduce the shear force on the contact surface [37, 38], which is less than the bonding force between polycrystals, and ultimately prevent deformation. If the shear force is less than the bonding force between polycrystals and larger than the bonding force between diamond and SiC [39], the damage will appear on the diamond coating on the textured surface.

4 Conclusions

In the present study, the cylindrical texture was prepared by laser fabricated on SiC substrate and modified with diamond (D/T-SiC) coating to improve tribological properties. In comparison, SiC, texture SiC (T-SiC), and diamond/SiC (D/SiC) were investigated under the same conditions. The structure, morphologies, and tribological properties in dry friction under various loads are analyzed, and the main conclusions were listed as follows:

1. The structure of the component of SiC did not change significantly after the laser texture, and a dense diamond coating with a crystal size of about 2.7 μm was deposited on the SiC.
2. Textured specimens (T-SiC, D/T-SiC) showed better tribological properties compared with flattened specimens (SiC, D/SiC), owing to the valley in the textured

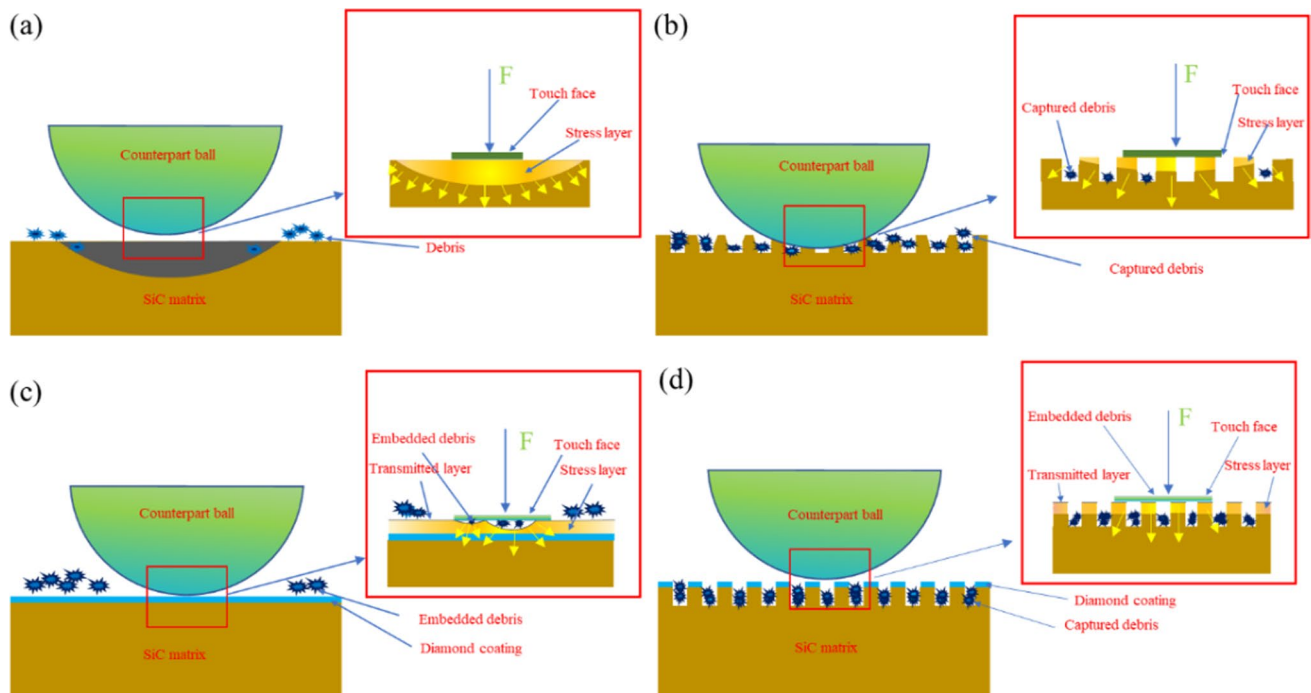


Fig. 15 Schematic diagram of wear mechanism for different specimens: **a** SiC, **b** T-SiC, **c** D/SiC, **d** D/T-SiC

specimens could store wear debris, eventually, decreased friction coefficient in tribological tests.

3. The deposited diamond layer plays a more important role than texture on the tribological properties. It supplies high load bearing, low friction coefficient, high wear resistance and deformation resistance.
4. The D/T-SiC specimen showed significantly lower friction coefficient at different applied loads (5 N, 15 N, and 25 N), about 79.7%, 84.8% and 86.2% compared with uncoated SiC, due to the ability of the surface to capture debris, together with the low friction nature of diamond. Additionally, the transition from diamond phase to sp²C on the counterpart ball, could decrease the friction and wear.

Acknowledgements The authors are grateful to Shanxi Provincial Natural Science Foundation (Grant No. 202203021211123), the Science and Technology Major Project of Shanxi (Grant No. 20181102013), and the fund of Shanxi “1331 Project” for financial support.

Availability of data and materials The data that support the findings of this study are available from the corresponding author upon reasonable request.

References

1. J. Kopac, P. Krajnik, High-performance grinding—a review. *J. Mater. Process. Technol.* **175**, 278–284 (2006). <https://doi.org/10.1016/j.jmatprotec.2005.04.010>
2. Q. An, J. Chen, W. Ming, M. Chen, Machining of SiC ceramic matrix composites: a review. *Chin. J. Aeronaut.* **34**, 540–567 (2021). <https://doi.org/10.1016/j.cja.2020.08.001>
3. T. Chen, J. Ji, Y. Fu, X. Yang, H. Fu, L. Fang, Tribological performance of UV picosecond laser multi-scale composite textures for C/SiC mechanical seals: theoretical analysis and experimental verification. *Ceram. Int.* **47**, 23162–23180 (2021). <https://doi.org/10.1016/j.ceramint.2021.04.312>
4. X. Li, H. Wang, B. Luo, The thermophysical properties and enhanced heat transfer performance of SiC-MWCNTs hybrid nanofluids for car radiator system. *Colloids Surf. A: Physicochem. Eng. Aspects* **612**, 125968 (2021). <https://doi.org/10.1016/j.colsurfa.2020.125968>
5. C.S. Ramesh, R. Noor Ahmed, M.A. Mujeebu, M.Z. Abdullah, Development and performance analysis of novel cast copper–SiC–Gr hybrid composites. *Mater. Des.* **30**, 1957–1965 (2009). <https://doi.org/10.1016/j.matdes.2008.09.005>
6. R. Meng, J. Deng, Y. Liu, R. Duan, G. Zhang, Improving tribological performance of cemented carbides by combining laser surface texturing and W-S-C solid lubricant coating. *Int. J. Refract. Metals Hard Mater.* **72**, 163–171 (2018). <https://doi.org/10.1016/j.ijrmhm.2017.12.024>
7. Z. Kang, Y. Fu, Y. Chen, J. Ji, H. Fu, S. Wang, R. Li, Experimental investigation of concave and convex micro-textures for improving anti-adhesion property of cutting tool in dry finish cutting. *Int. J. Precis. Eng. Manuf.-Green Technol.* **5**, 583–591 (2018). <https://doi.org/10.1007/s40684-018-0060-3>
8. S.-C. Vlădescu, A.V. Olver, I.G. Pegg, T. Reddyhoff, Combined friction and wear reduction in a reciprocating contact through laser surface texturing. *Wear* **358–359**, 51–61 (2016). <https://doi.org/10.1016/j.wear.2016.03.035>
9. Z. Wu, H. Bao, Y. Xing, L. Liu, Tribological characteristics and advanced processing methods of textured surfaces: a review. *Int. J. Adv. Manuf. Technol.* **114**, 1241–1277 (2021). <https://doi.org/10.1007/s00170-021-06954-2>
10. D. Kuo, J. Gui, B. Marchon, S. Lee, I. Boszormenyi, J.J. Liu, G.C. Rauch, S. Vierk, D. Meyer, Design of laser zone texture for low glide media. *IEEE Trans. Magn.* **32**, 3753–3758 (1996). <https://doi.org/10.1109/20.538826>
11. R. Bathe, V. Sai Krishna, S.K. Nikumb, G. Padmanabham, Laser surface texturing of gray cast iron for improving tribological behavior. *Appl. Phys. A* **117**, 117–123 (2014). <https://doi.org/10.1007/s00339-014-8281-y>
12. L.C. Tshabalala, S. Pityana, Surface texturing of Si₃N₄–SiC ceramic tool components by pulsed laser machining. *Surf. Coat. Technol.* **289**, 52–60 (2016). <https://doi.org/10.1016/j.surfcoat.2016.01.028>
13. B. Antoszewski, Mechanical seals with sliding surface texture—model fluid flow and some aspects of the laser forming of the texture. *Procedia Eng.* **39**, 51–62 (2012). <https://doi.org/10.1016/j.proeng.2012.07.007>
14. E.G. Orlova, D.V. Feoktistov, A.M. Abdelmagid, in: *Thermophysical basis of energy technologies (TBET 2020)* (2021)
15. P.W. May, CVD diamond: a new technology for the future? *Endeavour* **19**, 101–106 (1995). [https://doi.org/10.1016/0160-9327\(95\)97494-S](https://doi.org/10.1016/0160-9327(95)97494-S)
16. I.P. Hayward, Friction and wear properties of diamonds and diamond coatings. *Surf. Coat. Technol.* **49**, 554–559 (1991). [https://doi.org/10.1016/0257-8972\(91\)90116-E](https://doi.org/10.1016/0257-8972(91)90116-E)
17. S.V. Kidalov, F.M. Shakhov, Thermal conductivity of diamond composites. *Materials* (2009). <https://doi.org/10.3390/ma2042467>
18. Y. Xu, T. Wang, B. Chen, Y. Tang, Interface design to tune stress distribution for high performance diamond/silicon carbide coated cemented carbide tools. *Surf. Coat. Technol.* (2020). <https://doi.org/10.1016/j.surfcoat.2020.125975>
19. S. Yu, R. Wang, K. Zheng, J. Gao, X. Li, H. Hei, X. Liu, Z. He, Y. Shen, B. Tang, Influence of power density on high purity 63 mm diameter polycrystalline diamond deposition inside a 2.45 GHz MPCVD reactor. *J. Phys. D: Appl. Phys.* **49**, 355202 (2016). <https://doi.org/10.1088/0022-3727/49/35/355202>
20. J.F. Archard, Contact and rubbing of flat surfaces. *J. Appl. Phys.* **24**, 981–988 (1953). <https://doi.org/10.1063/1.1721448>
21. M. Olzon-Dionysio, M. Campos, M. Kapp, S. de Souza, S.D. de Souza, Influences of plasma nitriding edge effect on properties of 316L stainless steel. *Surf. Coat. Technol.* **204**, 3623–3628 (2010). <https://doi.org/10.1016/j.surfcoat.2010.04.034>
22. S. Gephart, J. Singh, A. Kulkarni, Structure–property relationship for sintered SiC by field assisted sintering technique. *Int. J. Refract. Metals Hard Mater.* **37**, 33–39 (2013). <https://doi.org/10.1016/j.ijrmhm.2012.10.013>
23. A. Pérez-Rodríguez, Y. Pacaud, L. Calvo-Barrío, C. Serre, W. Skorupa, J.R. Morante, Analysis of ion beam induced damage

- and amorphization of 6H-SiC by Raman scattering. *J. Electron. Mater.* **25**, 541–547 (1996). <https://doi.org/10.1007/BF02666633>
24. Z. Sun, J.R. Shi, B.K. Tay, S.P. Lau, UV Raman characteristics of nanocrystalline diamond films with different grain size. *Diam. Relat. Mater.* **9**, 1979–1983 (2000). [https://doi.org/10.1016/S0925-9635\(00\)00349-6](https://doi.org/10.1016/S0925-9635(00)00349-6)
 25. K. Miyoshi, Lubrication by diamond and diamondlike carbon coatings. *J. Tribol.* **120**, 379–384 (1998). <https://doi.org/10.1115/1.2834437>
 26. P.J. Blau, The significance and use of the friction coefficient. *Tribol. Int.* **34**, 585–591 (2001). [https://doi.org/10.1016/S0301-679X\(01\)00050-0](https://doi.org/10.1016/S0301-679X(01)00050-0)
 27. Z. Shi, Z. Jin, X. Guo, X. Shi, J. Guo, Interfacial friction properties in diamond polishing process and its molecular dynamic analysis. *Diam. Relat. Mater.* (2019). <https://doi.org/10.1016/j.diamond.2019.107546>
 28. P. Forquin, C. Denoual, C.E. Cottenot, F. Hild, Experiments and modelling of the compressive behaviour of two SiC ceramics. *Mech. Mater.* **35**, 987–1002 (2003). [https://doi.org/10.1016/S0167-6636\(02\)00321-6](https://doi.org/10.1016/S0167-6636(02)00321-6)
 29. J.B. Chen, Q.H. Fang, C.C. Wang, J.K. Du, F. Liu, Theoretical study on brittle–ductile transition behavior in elliptical ultrasonic assisted grinding of hard brittle materials. *Precis. Eng.* **46**, 104–117 (2016). <https://doi.org/10.1016/j.precisioneng.2016.04.005>
 30. M. Basista, D. Gross, The sliding crack model of brittle deformation: an internal variable approach. *Int. J. Solids Struct.* **35**, 487–509 (1998). [https://doi.org/10.1016/S0020-7683\(97\)00031-0](https://doi.org/10.1016/S0020-7683(97)00031-0)
 31. X. Zhao, R.M. Langford, I.P. Shapiro, P. Xiao, Onset plastic deformation and cracking behavior of silicon carbide under contact load at room temperature. *J. Am. Ceram. Soc.* **94**, 3509–3514 (2011). <https://doi.org/10.1111/j.1551-2916.2011.04674.x>
 32. Z. Zhang, W. Lu, W. Feng, X. Du, D. Zuo, Effect of substrate surface texture on adhesion performance of diamond coating. *Int. J. Refract. Metals Hard Mater.* **95**, 105402 (2021). <https://doi.org/10.1016/j.ijrmhm.2020.105402>
 33. C. Gao, M. Liu, Effects of normal load on the coefficient of friction by microscratch test of copper with a spherical indenter. *Tribol. Lett.* **67**, 8 (2018). <https://doi.org/10.1007/s11249-018-1124-9>
 34. M.Q. Ding, L. Li, C. Hua, J. Cai, J. Feng, in: 2019 International Vacuum Electronics Conference (IVEC), (2019), pp. 1–2. <https://doi.org/10.1109/IVEC.2019.8745254>
 35. Y.A.N. Liu, E.I. Meletis, Evidence of graphitization of diamond-like carbon films during sliding wear. *J. Mater. Sci.* **32**, 3491–3495 (1997). <https://doi.org/10.1023/A:1018641304944>
 36. G.C.A.M. Janssen, Stress and strain in polycrystalline thin films. *Thin Solid Films* **515**, 6654–6664 (2007). <https://doi.org/10.1016/j.tsf.2007.03.007>
 37. K. Sun, X. Fan, W. Zhang, P. Xue, D. Diao, Contact-focusing electron flow induced nanosized graphene sheet formation in amorphous carbon films for fast low-friction. *Carbon* **149**, 45–54 (2019). <https://doi.org/10.1016/j.carbon.2019.04.040>
 38. E. Liu, Y.F. Ding, L. Li, B. Blanpain, J.P. Celis, Influence of humidity on the friction of diamond and diamond-like carbon materials. *Tribol. Int.* **40**, 216–219 (2007). <https://doi.org/10.1016/j.triboint.2005.09.012>
 39. J. Du, L. Zhou, J. Li, Y. Yao, Analysis of chip formation mechanism in mill-grinding of SiCp/Al composites. *Mater. Manuf. Process.* **29**, 1353–1360 (2014). <https://doi.org/10.1080/10426914.2014.912309>

Publisher's Note Springer Nature remains neutral with regard to jurisdictional claims in published maps and institutional affiliations.

Springer Nature or its licensor (e.g. a society or other partner) holds exclusive rights to this article under a publishing agreement with the author(s) or other rightsholder(s); author self-archiving of the accepted manuscript version of this article is solely governed by the terms of such publishing agreement and applicable law.